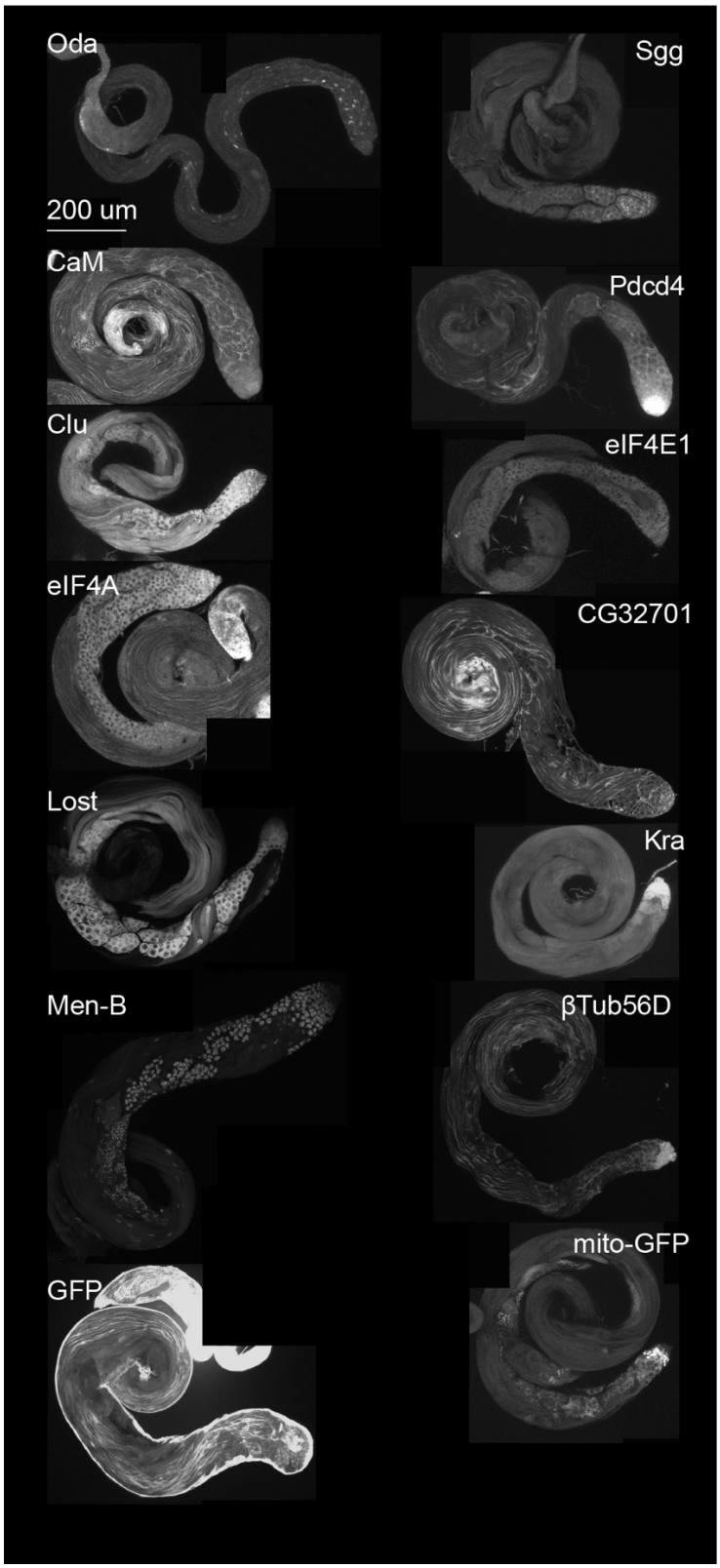

Figure S1. GFP expression pattern of FlyTrap lines used in FLIP imaging. Whole mount testes of each of the protein traps used for FLIP imaging to demonstrate differing patterns and levels of GFP expression. Non-FlyTrap lines expressing GFP and mito-GFP were also used.

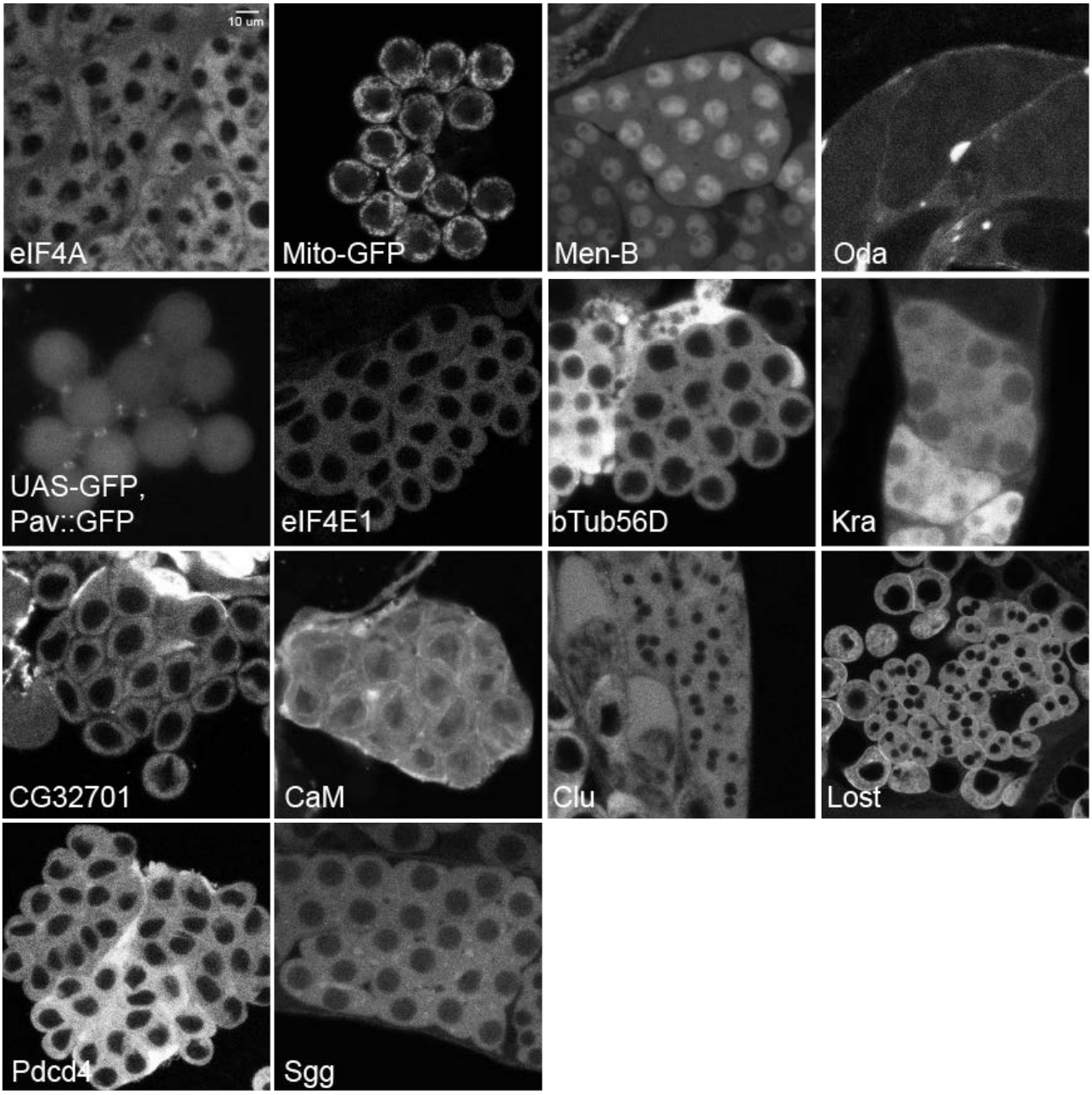

Figure S2. Expression in 16-cell cysts of all FlyTrap lines used for FLIP. Fixed examples of 16-cell cysts of each of the protein traps used for FLIP imaging to demonstrate differing patterns and levels of GFP expression. Non-FlyTrap lines expressing GFP and mito-GFP are also shown.

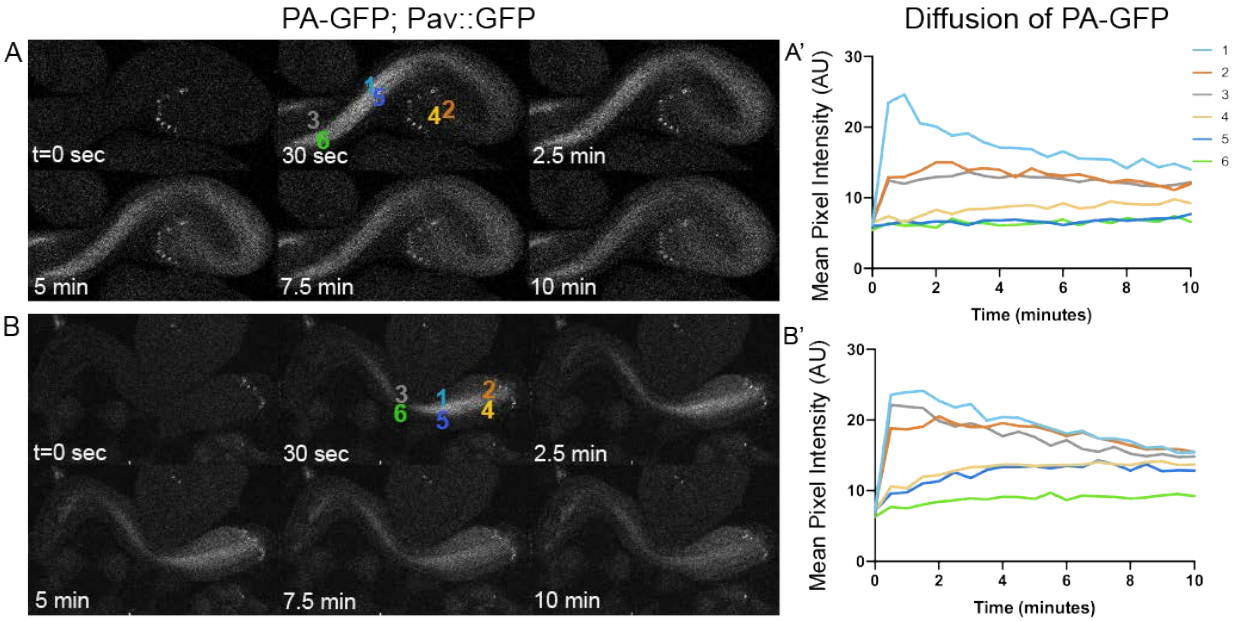

Figure S3. Movement of PA-GFP occurs through the RCs faster than through the tail perforations. (A-B) Still images of 10-minute movies capturing movement of PA-GFP in spermatid tails after activation in region 1. (A'-B') Quantification of PA-GFP fluorescence in several different locations along the spermatid tails show that PA-GFP is first observed near the RCs (region 4) rather than having traveled through the perforations (region 5).

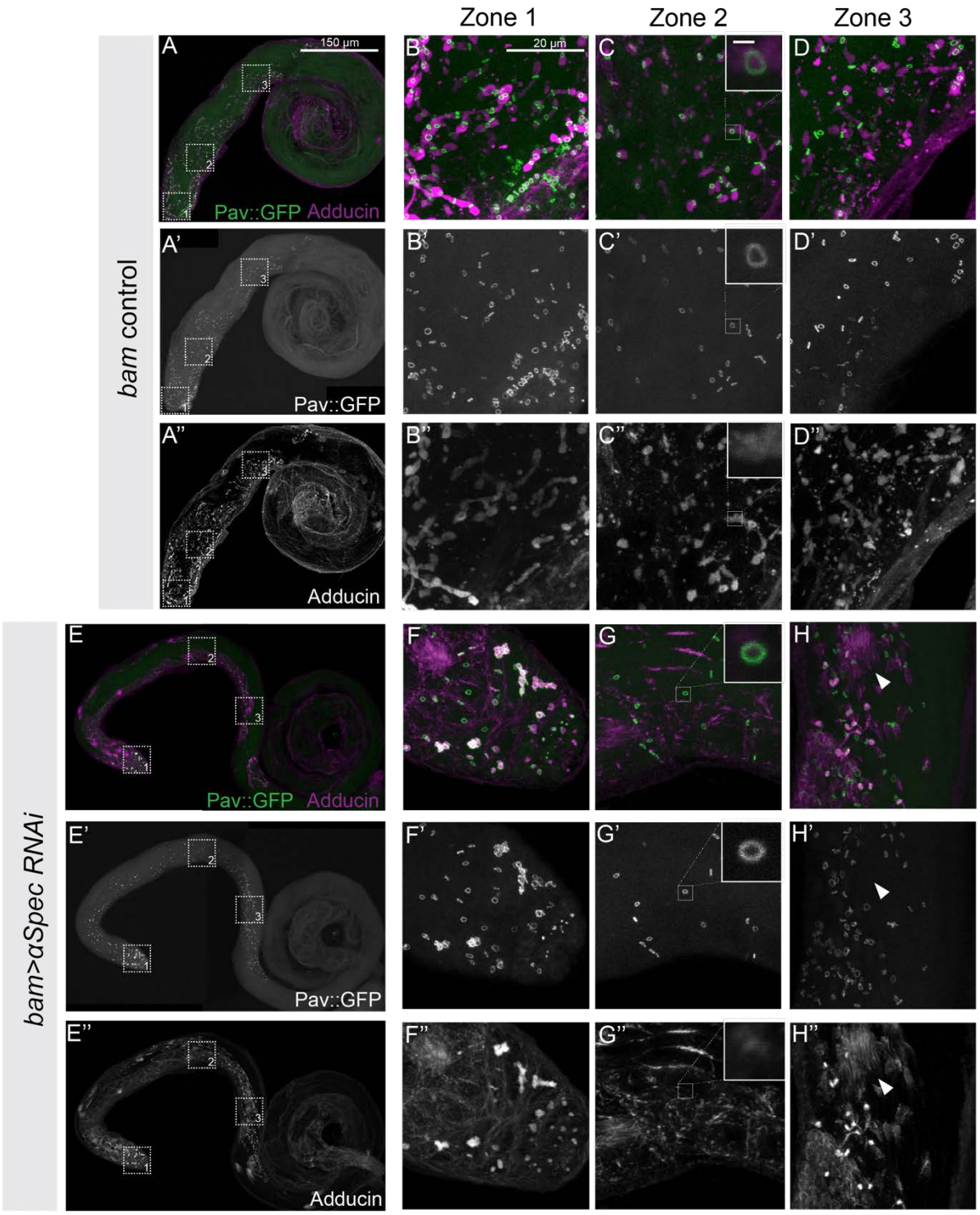

Figure S4. Fusome disruption by RNAi against α*Spectrin* using *bam-Gal4* (Adducin staining). (A) Wild-type testis with RCs marked by Pav::GFP and fusomes labeled with Adducin antibody (1B1). (B-D) Closeups of the regions marked by box in (A), highlighting the RCs (Pav, green) and fusome (Adducin, purple) in a wild-type testis in three different stages of development: mitotic (Zone 1), post-mitotic (Zone 2), and elongated spermatids (Zone 3). Insets in (C-C") highlight one RC, scale bar is 1 um. (E) Testes with α*Spectrin* RNAi lack Adducin staining at the fusome, but testis morphology appears unaffected. (F-H) Closeups of the regions marked in (E) showing Hts1B1 staining at the membrane rather than in a fusome pattern while Pav::GFP remained localized to the RCs. Small fusome-like fragments were observed in Zones 2 and 3.

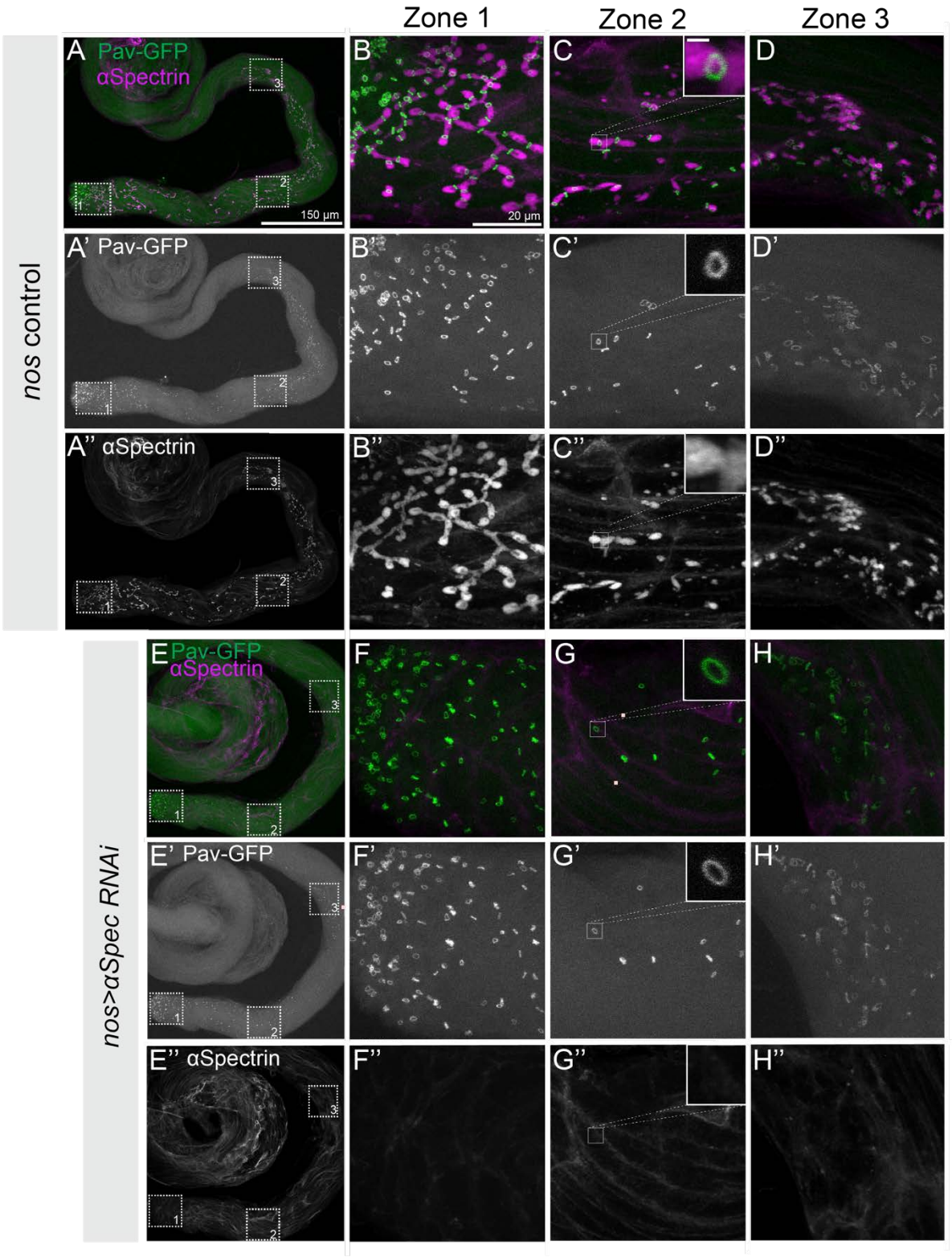

Figure S5. Fusome disruption by RNAi against α*Spectrin* using *nos-Gal4* (αSpectrin staining). (A) Wholemount Pav::GFP testis stained with αSpectrin antibody showed staining of the fusome similar to Hts1B1 (Adducin) antibody. (B-D) Close up of regions marked in (A) showing αSpectrin staining at wild-type RCs (B'-D') and the fusome (B"-D") at various stages of sperm development. (E) Disruption of fusome using *nos-Gal4>αSpectrin* RNAi showed a lack of αSpectrin staining at the fusome, but gross testis morphology appears unaffected. (F-H) Close up of insets from (E) showing intact RCs (F'-H') despite loss of αSpectrin staining (F"-H").)

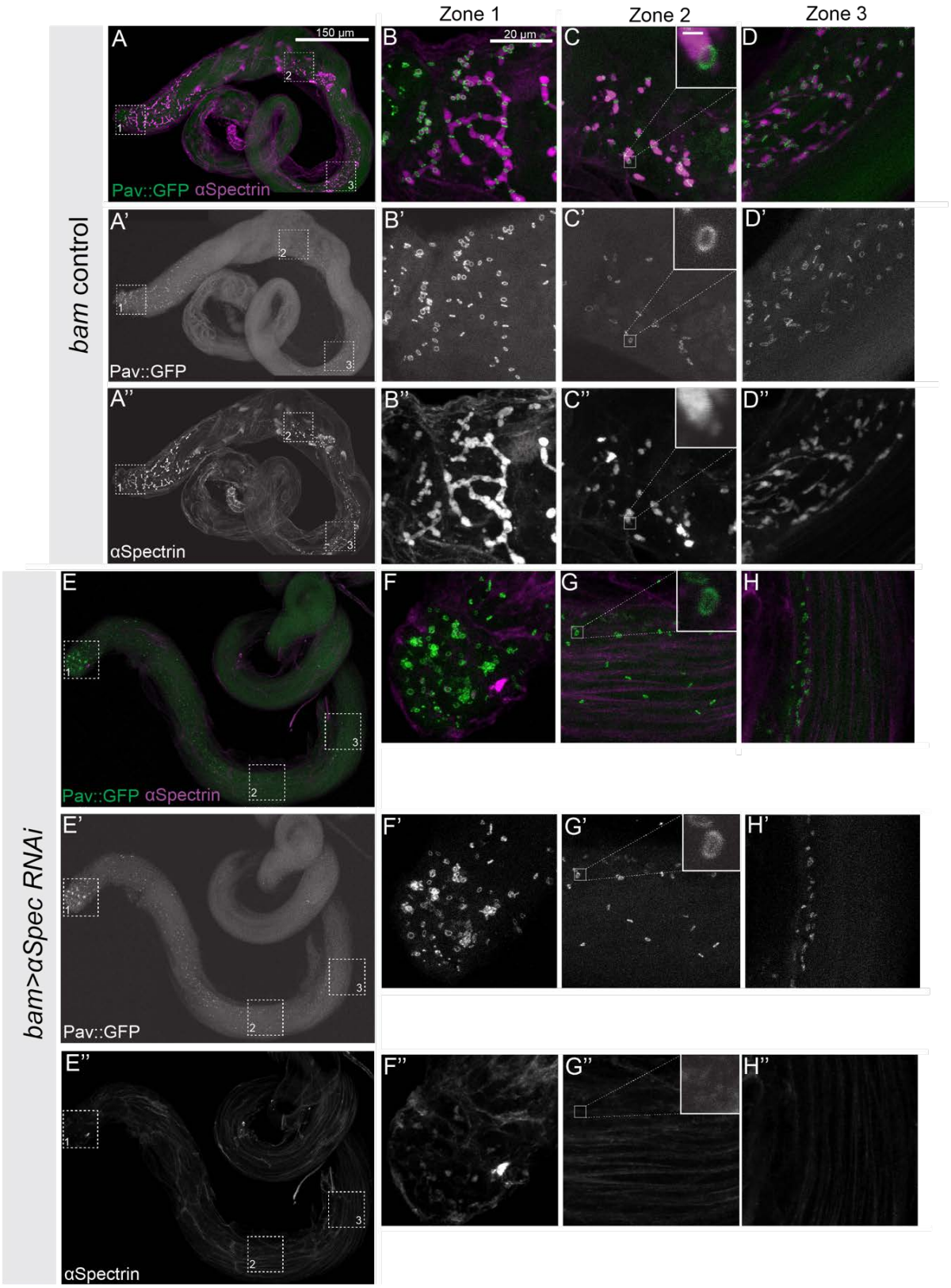

Figure S6. Fusome disruption by RNAi against α*Spectrin* using *bam-Gal4* (αSpectrin staining). (A) αSpectrin showed staining of the fusome similar to Hts1B1 (Adducin) antibody. (B-D) Close up of regions marked in (A) showing αSpectrin staining at wild-type RCs (B'-D') and the fusome (B"-D") at various stages of sperm development. (E) Disruption of fusome using *bam-Gal4>αSpectrin* RNAi showed a lack of αSpectrin staining at the fusome, but gross testis morphology appears unaffected. (F-H) Close up of insets from (E) showing intact RCs (F'-H') despite loss of αSpectrin staining (F"-H").

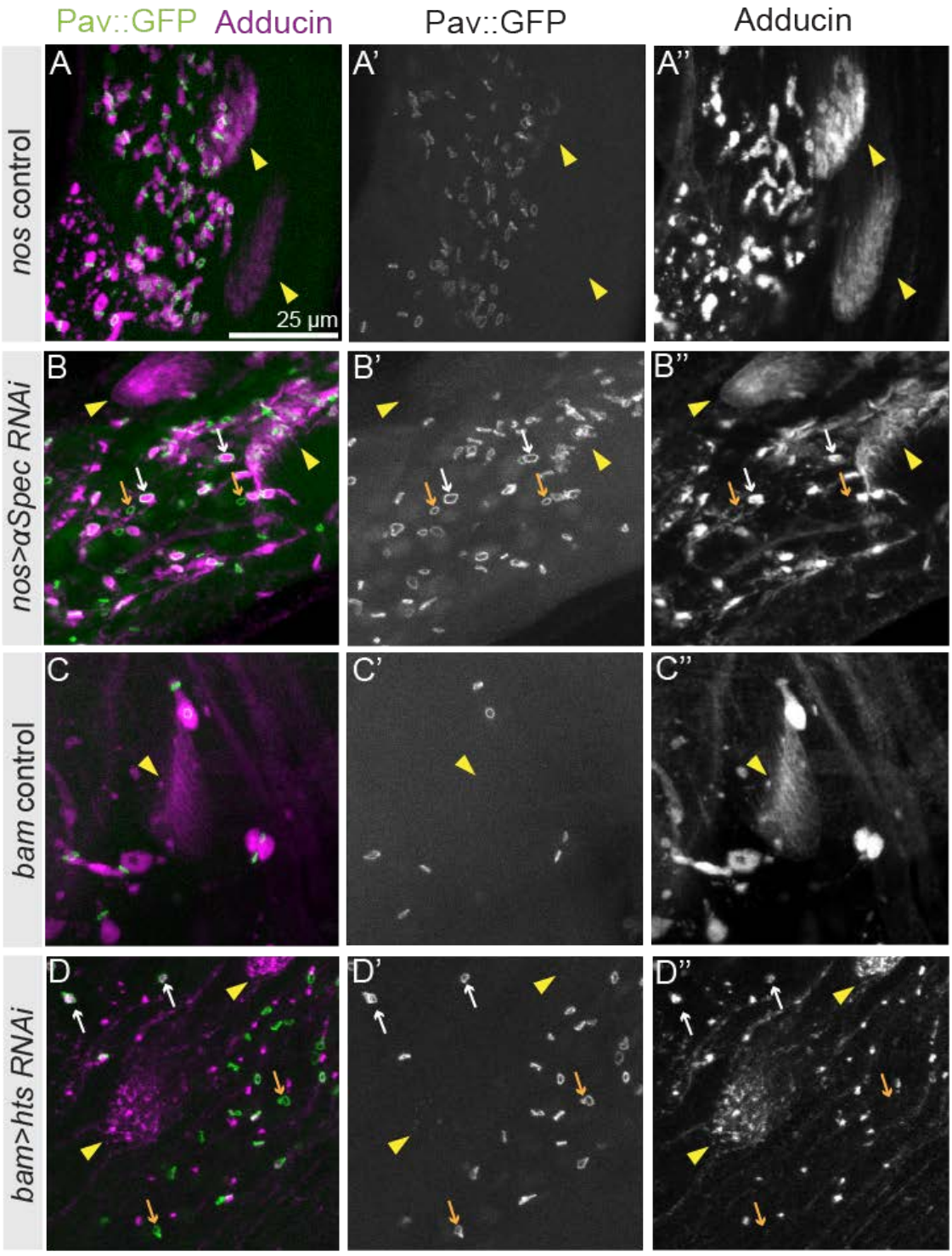

Figure S7. Knockdown of αSpec and Hts compromises the fusome but does not alter the localization of Adducin at elongating spermatid tails. Knockdown of αSpec and Hts compromises the fusome but does not alter the localization of Adducin at elongating spermatid tails. (A,C) *nos-Gal4* or *bam-Gal4* control testes (Zone 2) with RCs marked by Pav::GFP; fusomes and elongating spermatid tails (yellow arrowhead) labeled with Adducin antibody. (B) *nos>αSpec RNAi* testis showing fragmented fusomes and RCs that both associate with (white arrow) and fail to associate with (orange arrow) fusomes. (D) *bam>hts RNAi* testis showing fragmented fusomes and fragmented Adducin signal at the elongating spermatid tails. The majority of Pav::GFP-labeled RCs are not associated with the fusome fragments.

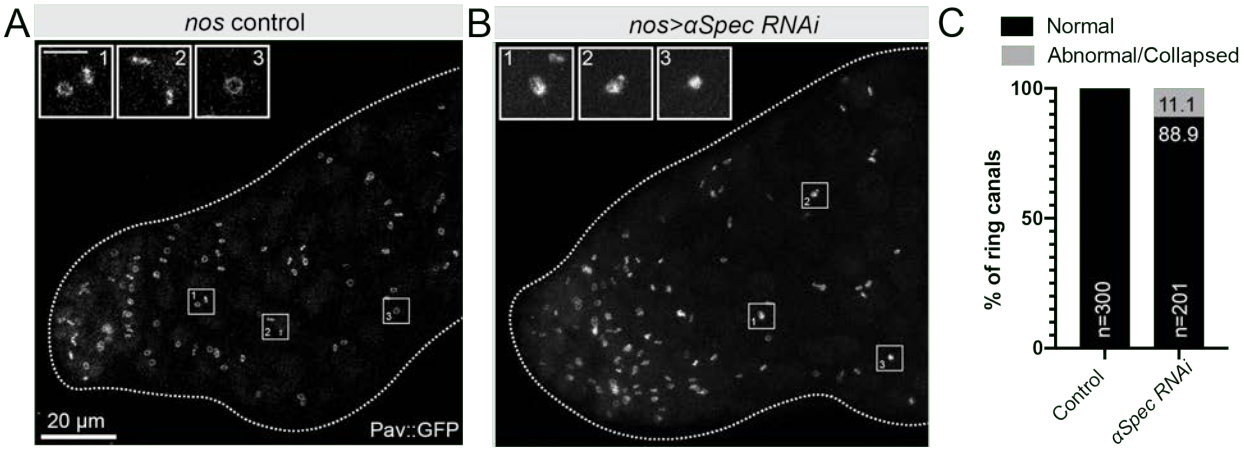

Figure S8. RC morphology following fusome knockdown (A, B). *nos-Gal4* control or *nos>aSpec RNAi* testes expressing Pav::GFP. (A) Boxed RCs are shown in the insets. Scale bar is 5 microns. (B) Abnormal or collapsed RCs highlighted in the insets. (C) Quantification of RC morphology.

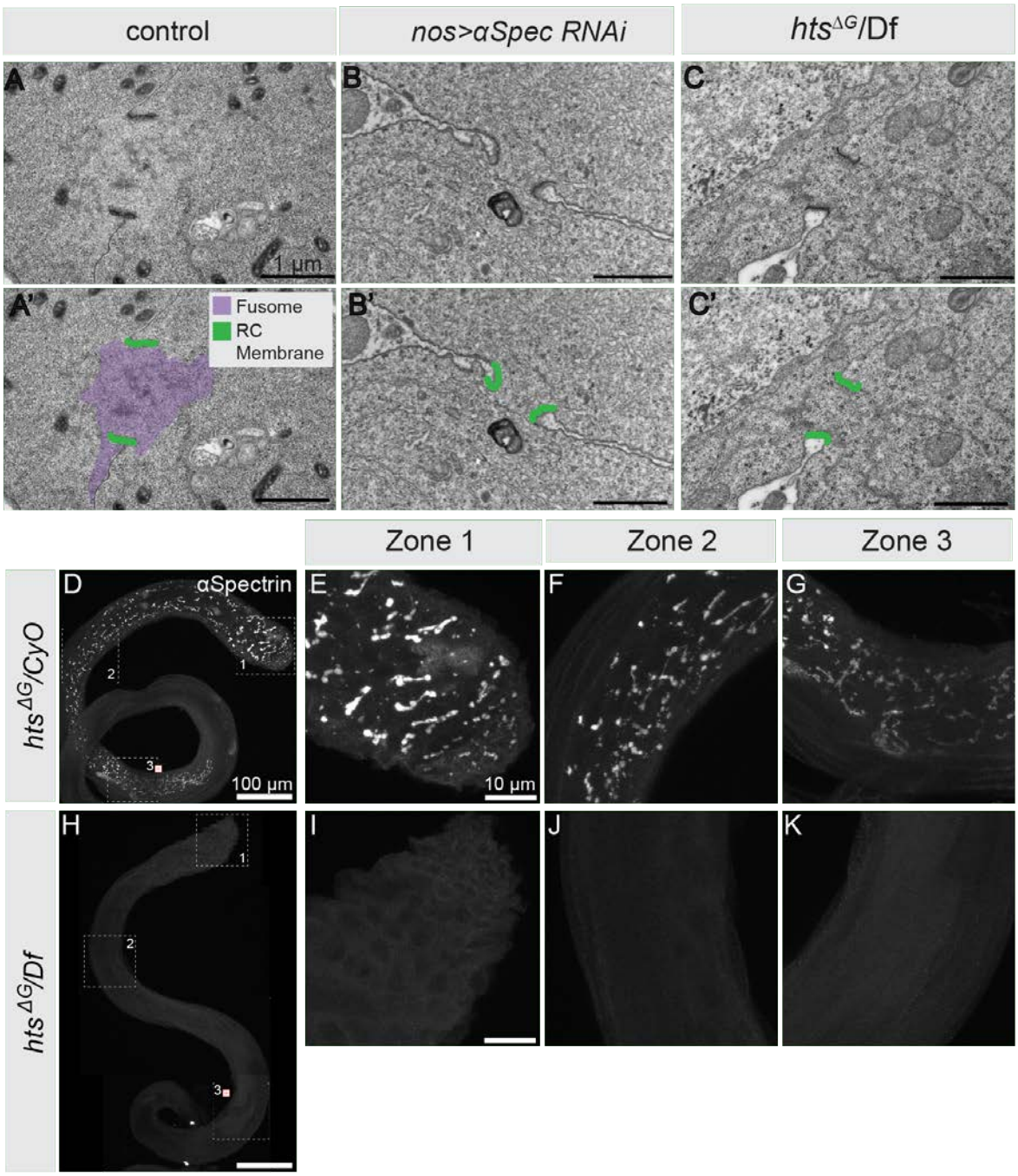

Figure S9. Additional EM showing clear fusome in wild type and compromised fusome in *αSpectrin* RNAi and *hts*$^{\Delta G}$ mutant testes. (A) EM of Pav::GFP testes showing RCs surrounding the fusome, a clear ribosome deficient cloud. (A') False coloring of (A) highlighting the fusome area (purple) and RCs (green). (B) EM pictures of *nos>αSpectrin* RNAi showing a lack of clearly marked fusome between the electron dense RCs. (C) EM images of *hts*$^{\Delta G}$*/Df* testes, which show no fusome structure but intact RCs. (D) Immunofluorescence of *hts*$^{\Delta G}$*/CyO* testis stained with *αSpectrin* antibody. (E-G) Insets from (D) highlighting the presence of the fusome in various stages of spermatogonial development. (H) Immunofluorescence of *hts*$^{\Delta G}$*/Df* shows a lack of *αSpectrin* staining at a fusome, but spermatogenesis and testis morphology appear unaffected. (I-K) Insets of (H) showing a distinct lack of *αSpectrin* antibody staining during mitotic, post-mitotic, and spermatid elongation stages.

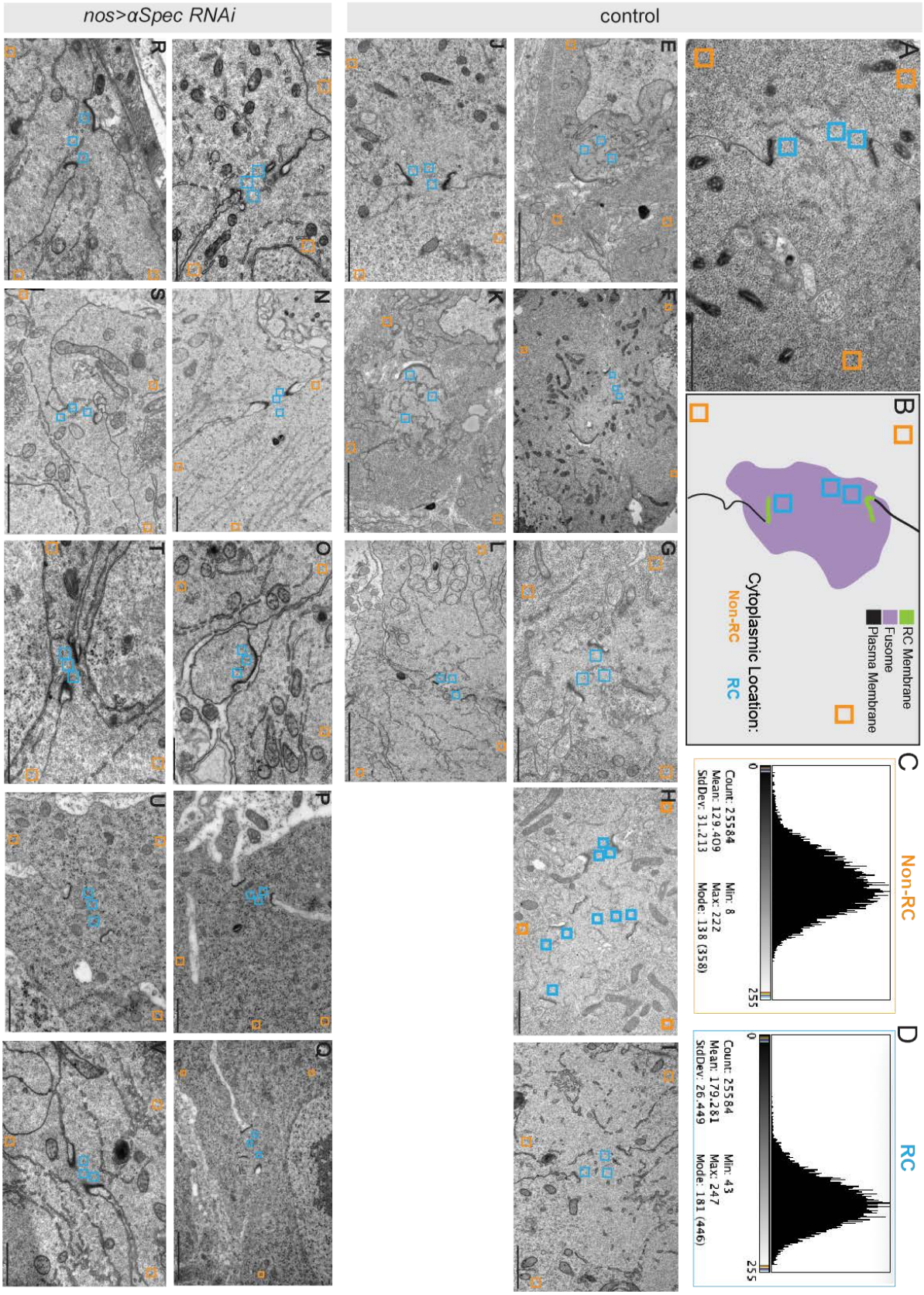

Figure S10. Additional TEM micrographs of control and *nos>aSpec RNAi* RCs. (A) Control RC with labeled ROIs (blue boxes mark RC cytoplasm; orange boxes mark non-RC cytoplasm) used for quantification of ribosome density. (B) Schematic of RC represented in (A) to mark the RC membrane (green), fusome (purple), plasma membrane (black). (C, D) Example histograms obtained from a single ROI in either the non-RC cytoplasm (orange) or RC cytoplasm (blue). (E-L) Electron micrographs of control RCs from which ribosome density measurements were obtained with labeled ROIs. (M) Electron micrographs of *nos>aSpec RNAi* RCs; measured ROIs are labeled.

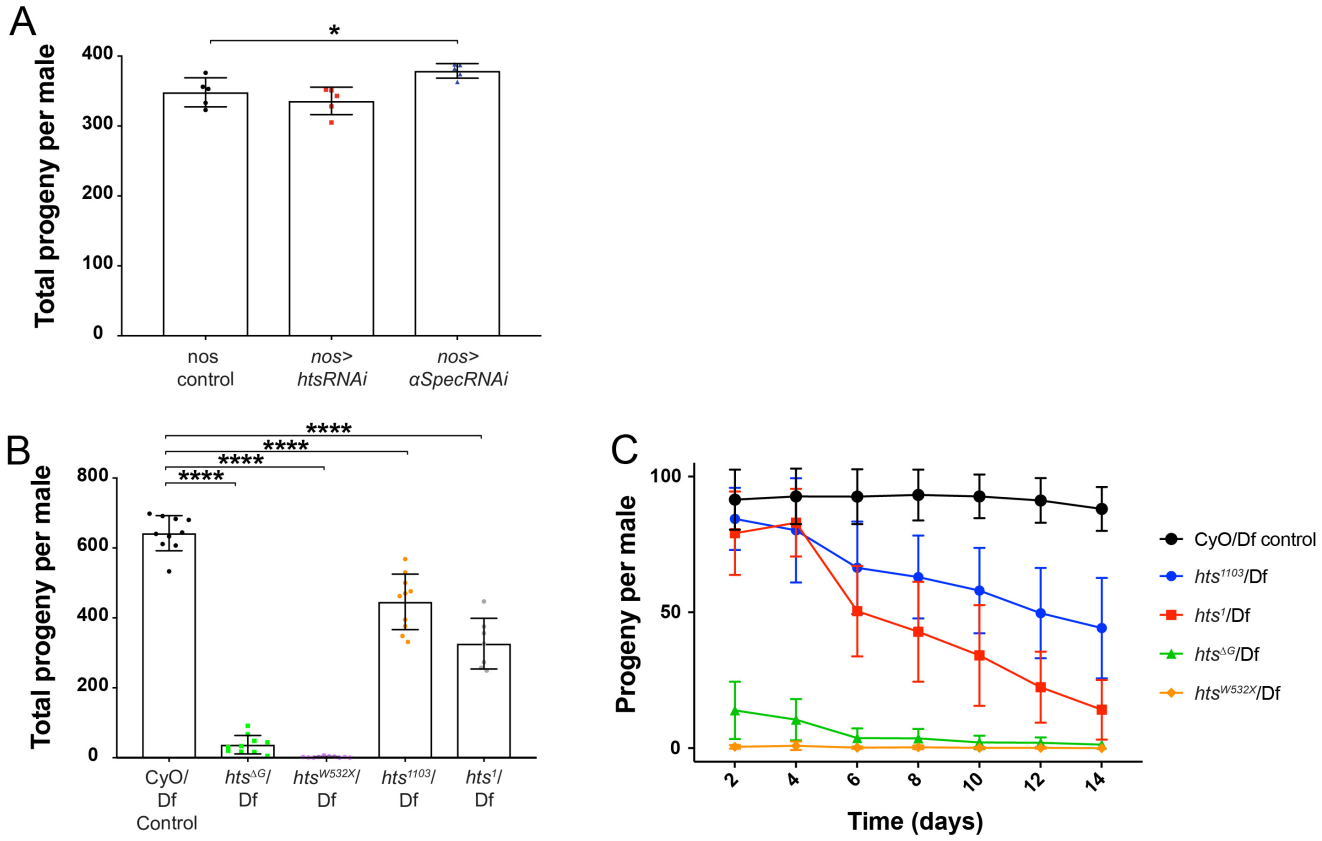

Figure S11. Fusome knockdown by germline specific RNAi does not have an effect on fertility. (A) Comparison of fertility (over a two-week period) as measured by total progeny per male between germline specific *nos-Gal4* control and *nos-Gal4* driving *hts* (p=0.45) or *αSpectrin* RNAi (p=0.03) showed a slight increase in fertility in the αSpectrin RNAi line. (B) Fertility assessment using hts alleles $hts^{\Delta G}$*/Df*, hts^{W532X}*/Df*, hts^{1103}*/Df* and hts^{1}*/Df* showed significant decrease in fertility compared to control (p<0.0001). (C) Fertility of hts^{1103}/Df and hts^{1}/Df decline over time in comparison to control. $hts^{\Delta G}$*/Df* and hts^{W532X}*/Df* were consistently less fertile than controls.

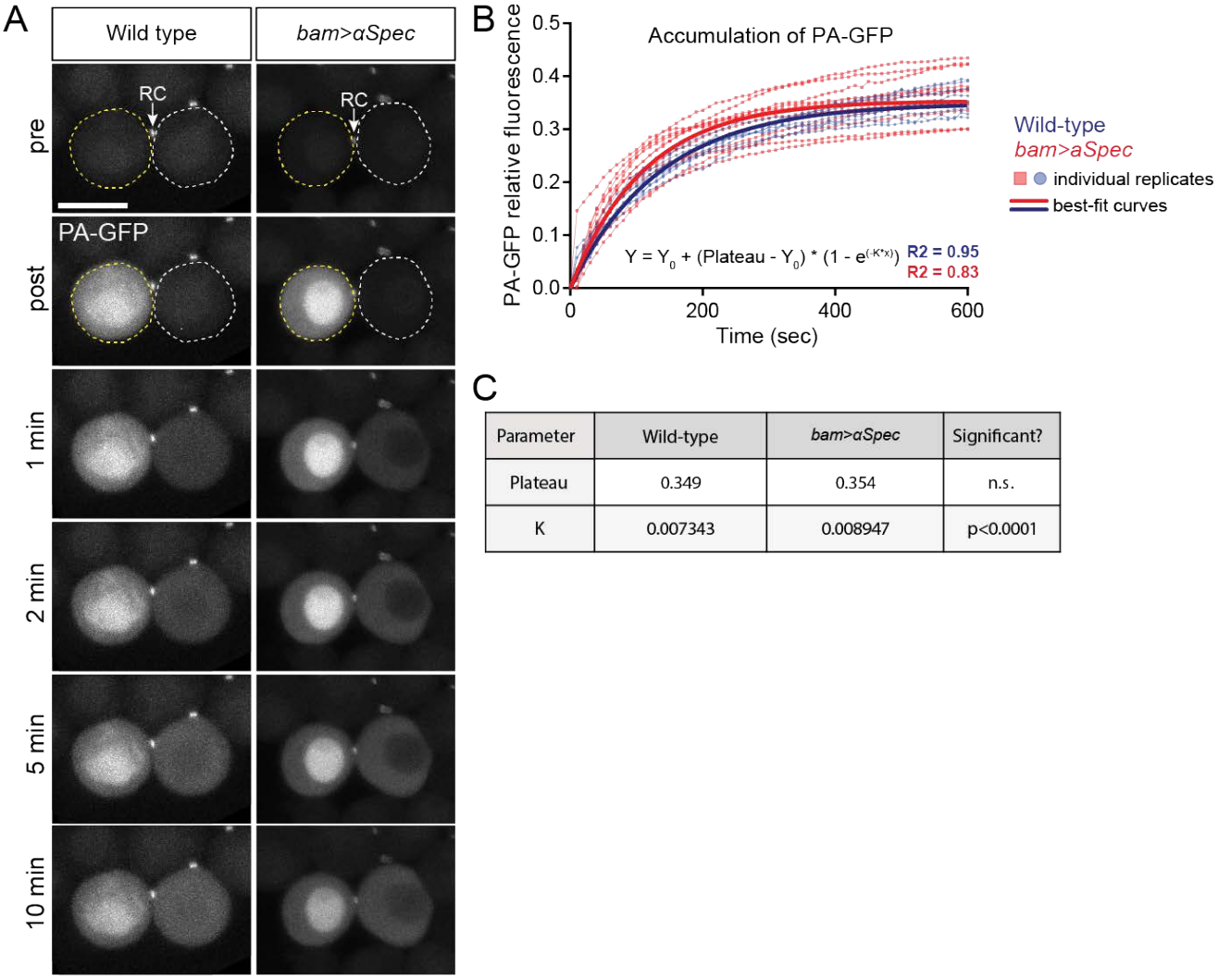

C

Parameter	Wild-type	*bam>αSpec*	Significant?
Plateau	0.349	0.354	n.s.
K	0.007343	0.008947	p<0.0001

Figure S12. Movement of PA-GFP through RCs in fusome-disrupted cells is faster than in wild-type cells. (A) A single cell expressing PA-GFP within a spermatocyte cyst was activated (yellow dashed outline) and PA-GFP fluorescence between the activated and recipient cell (white dashed outline) was imaged throughout a 10-minute time course in wild-type and fusome knockdown testes. Arrows indicate the RC, marked by Pav::GFP. Two-cell groups were selected for quantification, meaning that only movies in which PA-GFP diffused into a single adjacent cell were used for analysis. (B-C) Non-linear regression of PA-GFP RFU mean values (dashed lines) and fitted curves (solid lines) for both wild-type (blue lines) and fusome RNAi (red lines) testes. Both curves plateaued at the same RFU, but the rate of movement (as measured by the K rate constant parameter) in fusome RNAi was significantly faster than in wild-type ($p<0.0001$). wild-type: n=9; fusome RNAi: n=11. Scale bar = 20 μm.

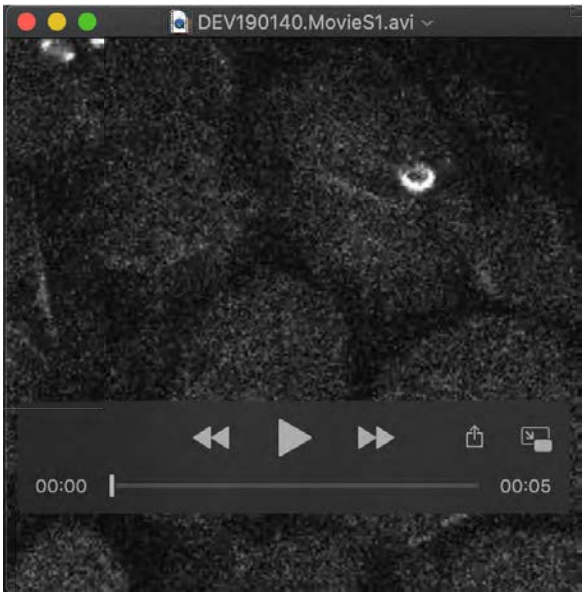

Movie 1: Movie showing movement of PA-GFP through the RCs in a 2-cell spermatogonial cyst. Photoactivation of PA-GFP in a single cell of two 2-cell spermatogonial cysts demonstrates intercellular exchange of cytoplasmic protein. Images were acquired at 30 second intervals for 10 minutes following activation.

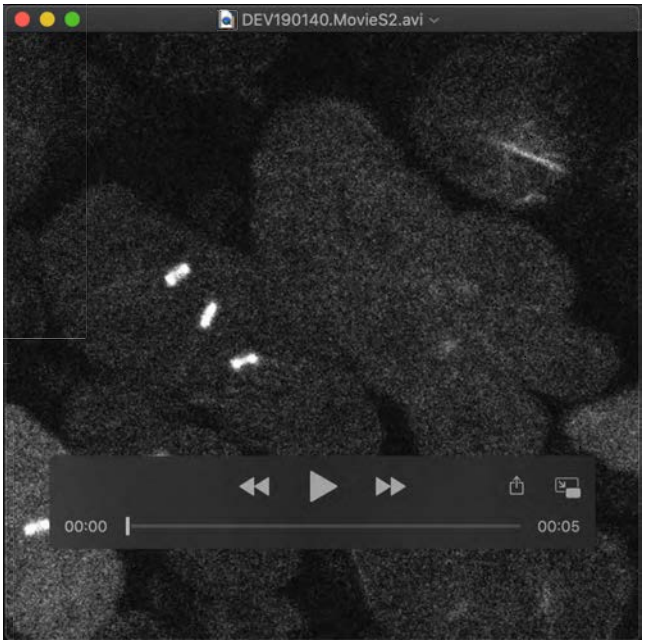

Movie 2: Movie showing movement of PA-GFP through the RCs in a 4-cell spermatogonial cyst. Photoactivation of PA-GFP in a single cell of a 4-cell spermatogonial cyst demonstrates rapid intercellular exchange of GFP. Images were acquired at 30 second intervals for 10 minutes following activation.

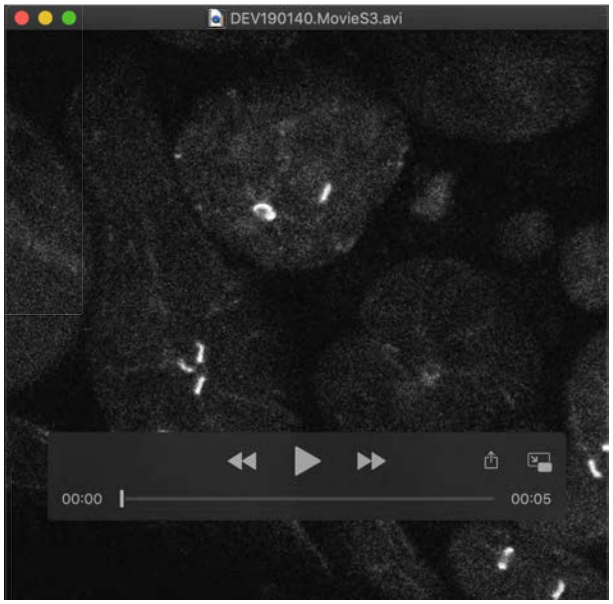

Movie 3: Movie showing movement of PA-GFP through the RCs in an 8-cell spermatogonial cyst. Photoactivation of PA-GFP in a single cell of an 8-cell spermatogonial cyst demonstrates intercellular exchange GFP through RCs in later stage mitotic cysts. Images were acquired at 30 second intervals for 10 minutes following activation.

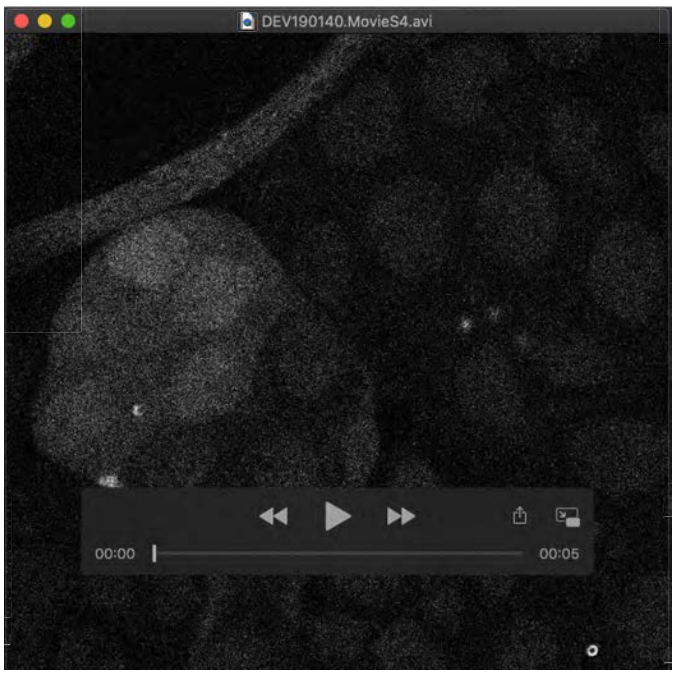

Movie 4: Movie showing movement of PA-GFP through the RCs in a 16-cell spermatocyte cyst. Photoactivation of PA-GFP in a single, center cell of a 16-cell primary spermatocyte cyst demonstrates intercellular exchange of cytoplasmic protein occurs even in cysts undergoing a growth phase. Images were acquired at 30 second intervals for 10 minutes following activation.

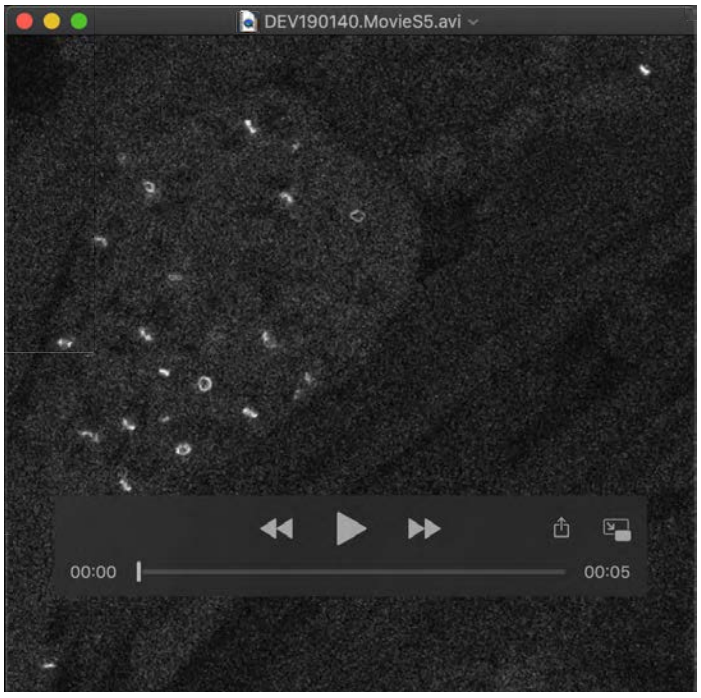

Movie 5: Movie showing movement of PA-GFP through the RCs in a 32-cell cyst. Photoactivation of PA-GFP in several cells of a 32-cell cyst demonstrates intercellular exchange of cytoplasmic protein happens during meiosis. Images were acquired at 30 second intervals for 10 minutes following activation.

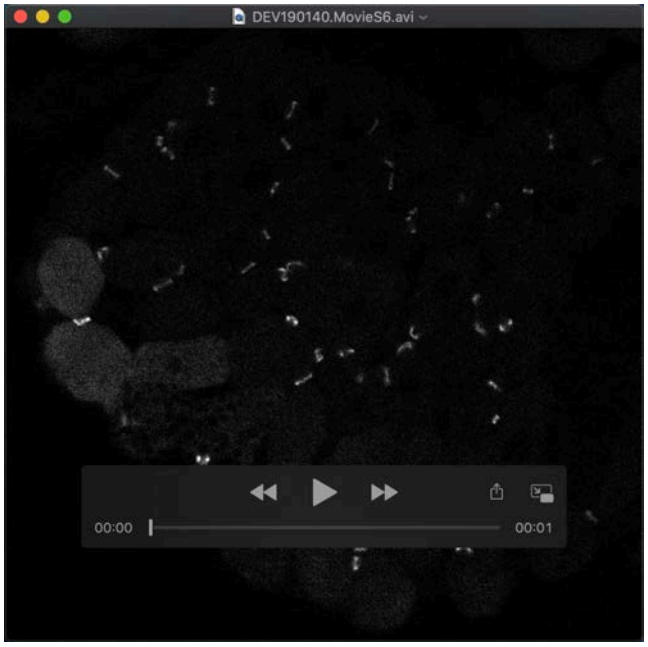

Movie 6: Movie showing movement of PA-GFP through the RCs in a 64-cell cyst. Photoactivation of PA-GFP in 2 single cells of a 64-cell post-meiotic cyst demonstrates protein exchange occurs post-meiotically. Images were acquired at 30 second intervals for 10 minutes following activation.

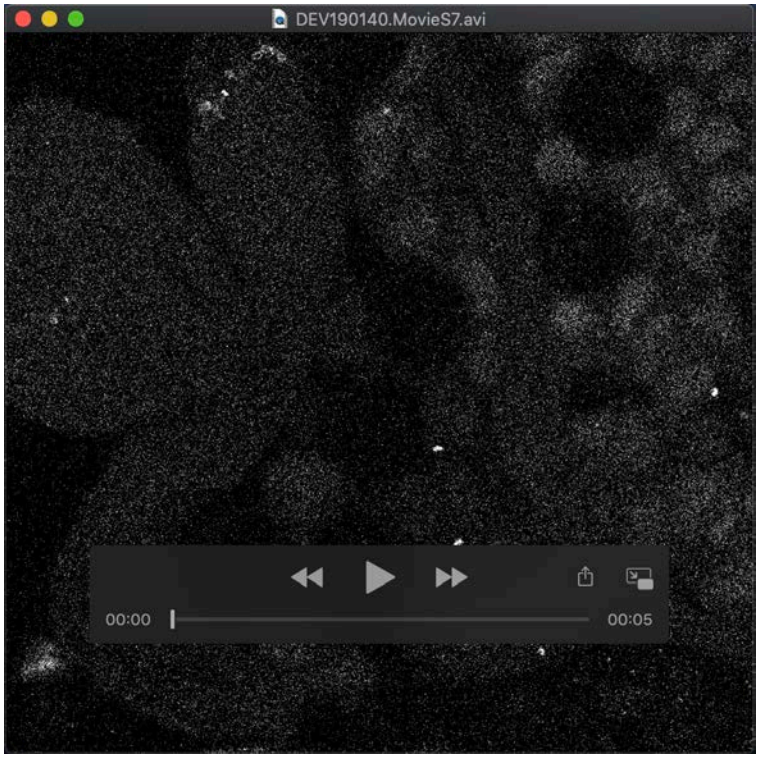

Movie 7: Movie showing movement of PA-GFP through the RCs in elongating spermatids. Photoactivation of PA-GFP in a subset of spermatids demonstrates intercellular exchange of cytoplasmic protein occurs post-tail elongation. Images were acquired at 30 second intervals for 10 minutes following activation.

Movie 8: Moving showing movement of PA-GFP through the RCs in 2- and 4-cell spermatogonial cysts lacking a fusome. Photoactivation of PA-GFP in single cells of 2- and 4-cell spermatogonial cysts in *nos-Gal4>αSpectrin* RNAi testes demonstrates intercellular exchange of cytoplasmic protein occurs despite the lack of fusome structure. Images were acquired at 30 second intervals for 10 minutes following activation.

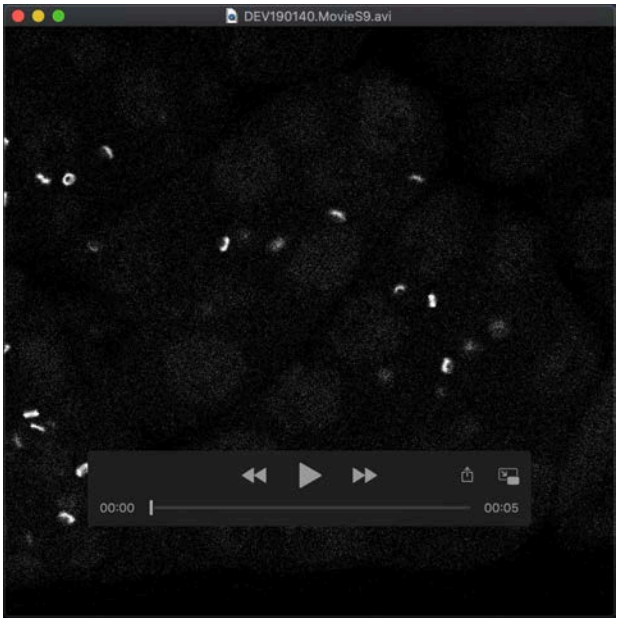

Movie 9: Movie showing movement of PA-GFP through the RCs in a 16-cell spermatocyte cyst lacking a fusome. Photoactivation of PA-GFP in a single cell of 16-cell spermatocyte cyst in *bam-Gal4>αSpectrin* RNAi testes demonstrates intercellular exchange of PA-GFP is not mediated by the fusome in primary spermatocytes. Images were acquired at 30 second intervals for 10 minutes following activation.

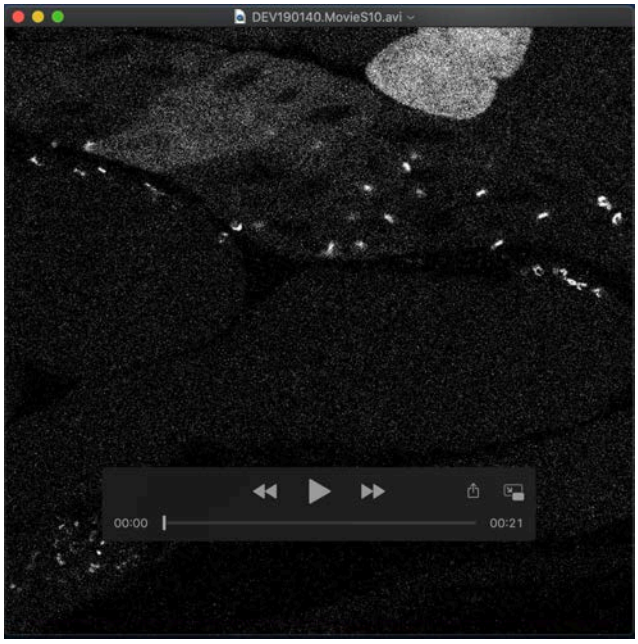

Movie 10: Movie showing movement of PA-GFP through the RCs in a spermatids lacking a fusome. Photoactivation of PA-GFP in a subset of spermatids in *bam-Gal4>αSpectrin* RNAi testes demonstrates intercellular exchange of PA-GFP is not mediated by the fusome post-meiotically. Images were acquired at 30 second intervals for 40 minutes following activation.

Table S1. Reagents

REAGENT or RESOURCE	SOURCE	IDENTIFIER
Antibodies		
Mouse monoclonal anti-Hts (1B1)	Developmental Studies Hybridoma Bank	Cat#1b1, RRID:AB_528070
Mouse monoclonal anti-αSpec (3A9)	Developmental Studies Hybridoma Bank	Cat#3A9 (323 or M10-2), RRID:AB_528473
Goat anti-mouse IgG Secondary Antibody, Alexa Fluor 568	Thermo Fisher Scientific	Cat#A-11031, RRID: AB_144696
Chemicals and Recombinant Protein		
Paraformaldehyde, 16% solution, EM grade	VWR	Cat#15710-S
Bovine Serum Albumin	AmericanBio	Cat#AB01088
Triton X-100	AmericanBio	Cat#AB02025-00500
ProLong Gold Antifade Mountant	Thermo Fisher Scientific	Cat#P36934
Aqua-Poly/Mount	Polysciences, Inc.	Cat#18606
Experimental Models		
D. melanogaster: pJFRC92-20XUAS-IVS-Syn21-mC3PAGFP-p10	Laboratory of G. Rubin; Pfeiffer et al. 2012	N/A
D. melanogaster: Bam-Gal4: W1118; P[Bam-Gal4:VP16]	Labortory of D. McKearin; Chen & McKearin 2003	N/A
D. melanogaster: htsΔG	Zuker collection, Koundakjian et al., 2004	FlyBase ID: FBal0212993
D. melanogaster: Tub-Gal4: y1 w*; P{w+mC=tubP-GAL4}LL7/TM3, Sb1 Ser1	Bloomington Drosophila Stock Center	RRID:BDSC_5138
D. melanogaster: Nos-Gal4: P{w+mC=GAL4::VP16-nos.UTR}MVD2, w1118	Bloomington Drosophila Stock Center	RRID:BDSC_7303
D. melanogaster: αSpectrin shRNA: y1 sc* v1; P{y+t7.7 v+t1.8=TRiP.HMC04371}attP40	Bloomington Drosophila Stock Center	RRID:BDSC_56932
D. melanogaster: hts Df: w[1118]; Df(2R)BSC135/CyO	Bloomington Drosophila Stock Center	RRID: BDSC_9423
D. melanogaster: y[1] M{RFP[3xP3.PB] GFP[E.3xP3]=vas-int.Dm}ZH-2A w[*]; PBac{y[+]-attP-3B}VK00037	Bloomington Drosophila Stock Center	RRID:BDSC_24872
D. melanogaster: JFRC81- 10XUAS-IVS-Syn21-GFP-p10	Laboratory of G. Rubin; Pfeiffer et al. 2012	N/A
D. melanogaster: Cam::GFP	Laboratory of L. Cooley; Kelso et al. 2004	YC0069LE
D. melanogaster: Clu::GFP: w1118; P{w+mC=PTT-GA}cluG00271	Bloomington Drosophila Stock Center	RRID:BDSC_6842
D. melanogaster: EIF4α::GFP	Laboratory of L. Cooley; Kelso et al. 2004	YC0001
D. melanogaster: EIF4E1::GFP: y1 w*/Dp(1;Y)y+; P{w+mC=PTT-GC}eIF4E1YC0001	Bloomington Drosophila Stock Center	RRID:BDSC_50858
D. melanogaster: G0320::GFP: w* P{w+mC=PTT-un1}l(1)G0320^{G00024}	Bloomington Drosophila Stock Center	RRID:BDSC_50839
D. melanogaster: Lost::GFP: w1118; P{w+mC=PTT-GA}lostZCL3169	Bloomington Drosophila Stock Center	RRID:BDSC_6832
D. melanogaster: Mito::GFP: w1118; P{w+mC=UAS-mito-HA-GFP.AP}2/CyO	Bloomington Drosophila Stock Center	RRID:BDSC_8442
D. melanogaster: Pdcd4::GFP: w1118 P{w+mC=PTT-GB}Pdcd4G93	Bloomington Drosophila Stock Center	RRID:BDSC_38446
D. melanogaster: Sgg::GFP: y1 P{w+mC=PTT-un1}sggZCL1912 w*	Bloomington Drosophila Stock Center	RRID:BDSC_50887
D. melanogaster: Kra::GFP: y1 w*; l(2)**/In(2LR)Gla, wgGla-1; PBac{y+mDint2=HpaI-GFP.A}kraYD0086/TM6C, Sb1	Bloomington Drosophila Stock Center	RRID:BDSC_50873
D. melanogaster: Men-B::GFP: w*; l(2)**/In(2LR)Gla, wgGla-1; P{w+mC=PTT-GB}Men-bYB0142	Bloomington Drosophila Stock Center	RRID:BDSC_50854
D. melanogaster: Oda::GFP	Laboratory of L. Cooley; Kelso et al. 2004	YD0523
D. melanogaster: βTub56D::GFP: w*; P{w+mC=PTT-GC}betaTub56DYC0063/CyO	Bloomington Drosophila Stock Center	RRID:BDSC_50867
Oligonucleotides		
Primer for HA::KnSm::FLAG (forward): TACCCCTACGACGTGCCCGACTACGCCatctggacaagggaaaacg	This study	N/A
Primer for HA::KnSm::FLAG (reverse): CTTATCGTCATCATCCTTGTAATCatctcgtgatggcaggttg	This study	N/A
Primer for HA::GFP::FLAG (forward): TACCCCTACGACGTGCCCGACTACGCCATGTCCAAAGGTGAAGAACTG	This study	N/A
Primer for HA::GFP::FLAG (reverse): TTACTTATCGTCATCATCCTTGTAATCCTTGTAGAGCTCATCCATGC	This study	N/A
Primer for insertion of KnSm cassette and HA::GFP::FLAG at the Pav c-terminus for Pav::GFP BAC transgene (forward): CCCGCTGCAATCTCGGCATTGAGGGACACAGCAGCAAGAAGTCGAAAATCTACCCCTACGACGTGCCC	This study	N/A
Primer for insertion of KnSm cassette and HA::GFP::FLAG at the Pav c-terminus for Pav::GFP BAC transgene (reverse): CTATGAACTAAATGGGTAATTGACTTTGAGAATTCCACGCTGAGTCATTTTTACTTATCGTCATCATCCTTG	This study	N/A
Recombinant DNA		
BAC CH322-102N03	CHORI	N/A
Software		
ImageJ/FIJI	NIH	https://fiji.sc/
Prism 7	GraphPad	https://www.graphpad.com/scientificsoftware/prism/
Imaris 9.0	Bitplane	http://www.bitplane. com/
Other		
Drosophila transgenesis: site-specific integration	Rainbow Transgenic Flies, Inc.	http://www.rainbowgene.com/